Surface-Directed Phase Separation via a Two-Step Quench Process in Binary Polymer Mixture Films with Asymmetry Compositions

ARTICLE *in* THE JOURNAL OF PHYSICAL CHEMISTRY B · AUGUST 2008

Impact Factor: 3.3 · DOI: 10.1021/jp801648t · Source: PubMed

4 AUTHORS, INCLUDING:

Xu-Ming Xie
Tsinghua University
168 PUBLICATIONS **1,590** CITATIONS

SEE PROFILE

Article

Surface-Directed Phase Separation via a Two-Step Quench Process in Binary Polymer Mixture Films with Asymmetry Compositions

Li-Tang Yan, Jialin Li, Fengbo Zhang, and Xu-Ming Xie

J. Phys. Chem. B, **2008**, 112 (29), 8499-8506 • DOI: 10.1021/jp801648t • Publication Date (Web): 27 June 2008

Surface-Directed Phase Separation via a Two-Step Quench Process in Binary Polymer Mixture Films with Asymmetry Compositions

Li-Tang Yan,*,† Jialin Li, Fengbo Zhang, and Xu-Ming Xie*

Advanced Materials Laboratory, Department of Chemical Engineering, Tsinghua University, Beijing 100084, People's Republic of China

Received: February 25, 2008; Revised Manuscript Received: May 13, 2008

Surface-directed phase separation via a two-step quench process in asymmetry polymer mixtures is numerically investigated by coupling the Flory−Huggins−de Gennes equation with the Cahn−Hilliard−Cook equation. Two distinct situations, i.e., the minority component is preferred by the surface and the majority component is preferred by the surface, are discussed, respectively. The morphology and evolution dynamics of the phase structure, especially the secondary domain structure, are analyzed. The wetting layer formation mechanisms during the two-step quench process are examined. The simulated results demonstrate that different secondary domain structures in these two situations can be induced by the second quench with deeper quench depth, which can be used to tailor phase morphology. It is also found that, in the second quench process, the evolution of the wetting layer thickness can cross over to a faster growth when the preferential component is the minority component. In this situation, the formation mechanism of the wetting layer will change and is eventually determined by the second quench depth. However, when the preferential component is the majority component, a deeper second quench depth corresponds to a slower growth of the wetting layer thickness. The chemical potential is calculated to explain the difference regarding the growth dynamics of the wetting layer thickness between these both situations.

1. Introduction

The films of polymer blends have received much attention because of their technological importance in dielectrics, photoresists, optics, lubrication, adhesives, and others. In recent years, the effect of surfaces on the phase separation in these films has become a focus of research.[1,2] It is often the case that a surface has a preferential attraction for one of the components, when the phase morphology and evolution dynamics can be dramatically altered by the wetting phenomena for the surface.[2–4] Typically, when the mixture is quenched below the coexistence curve, a wetting layer of the preferential component forms near the surface simultaneously, and an anisotropic wave occurs near the wetting layer and propagates into the bulk. In this case, the mixture really undergoes two dynamic processes, i.e., bulk phase separation and wetting layer growth, which is referred to as surface-directed phase separation (SDPS).[2,3a] In this problem, an interesting interplay occurs between the surface potential and the bulk chemical potential, leading to different formation mechanisms of the wetting layer.[3c,4d,e,5] Generally speaking, when the composition concentration is changed[4d,e] and/or the quench depth gets deeper,[5] the growth of wetting layer thickness R_1 with time t can exhibit three laws, i.e., a pure diffusion-limited growth law ($R_1 \propto t^{1/2}$), a logarithmic growth law ($R_1 \propto \ln(t)$), and the Lifshitz−Slyozov (LS) growth law ($R_1 \propto t^{1/3}$). In consequence, with the anisotropic wave induced by the surface potential penetrating into the bulk, the near-surface domain structure will be altered and the overall morphology of the film will be different from the respective bulk situation.[3–5]

The previous studies regarding the phase dynamics and the wetting layer formation mechanisms of SDPS generally concern mixtures with one-step quench process, in which the mixture is quenched from the one-phase region to a certain point in the unstable region of the phase diagram.[2–5] However, the inconstant temperature is more common in experiment and technology. Thus, the study of SDPS with a various thermal history is really a very important topic. The simplest but most important thermal history for the polymer blends mixture is the two-step quench process, in which the mixture following a one-step quench process is sequentially quenched into the other point with a deeper quench depth.[6] Actually, the phase separation of a general polymer blend mixture via the two-step quench process has been investigated experimentally[6,7] and theoretically.[8] These works demonstrate that the phase morphology and dynamics via a two-step quench process have much difference from that via a one-step quench process. Its typical character is that, during the initial stage following a second quench, secondary domains appear briefly in the primary domains obtained from the first quench depth.[6–8] It can be imagined that the novel phase morphology and evolution dynamics may be observed if a surface effect is coupled into the polymer mixture via a two-step quench process. However, there is almost no data on the two-step phase separation of the polymer mixture near a preferential surface. The question as to what precedes the wetting layer formation mechanism in the two-step SDPS is still an open one. Moreover, whether new phase morphologies in the bulk can be induced in the two-step SDPS has been unclear even up to now.

We numerically concern the important topics by coupling the Flory−Huggins−de Gennes (FHdG) equation with the Cahn−Hilliard−Cook (CHC) equation. In the present paper, we first introduce the two-step SDPS in asymmetry polymer mixtures.

* Corresponding authors. E-mail: li-tang.yan@uni-bayreuth.de (L.-T.Y.), xxm-dce@mail.tsinghua.edu.cn (X.-M.X.).

† Current address: Department of Physical Chemistry II, Universität Bayreuth, D-95440 Bayreuth, Germany.

10.1021/jp801648t CCC: $40.75
Published on Web 06/27/2008

Two distinct situations, i.e., the minority component is preferred by the surface and the majority component is preferred by the surface, are discussed, respectively. The morphology and evolution dynamic of the phase structure, especially the secondary domain structure, are analyzed in detail. The changes of the wetting layer formation mechanism during the two-step quench process are also examined.

2. Model and Numerical Procedure

The CHC equation, appropriate to an incompressible binary mixture, is employed to model the dynamics of the SDPS with binary mixtures (A and B), which can be written as[9]

$$\frac{\partial \varphi}{\partial t} = M\nabla^2 \frac{\delta F\{\varphi(r,t)\}}{\delta \varphi(r,t)} + \eta(r,t) \quad (1)$$

where $\phi(r, t)$ is the local fraction of component A at point r at time t. The same degree of polymerization, $N_A = N_B = N$, is set for a symmetric binary mixture. M is a phenomenological parameter characterizing the self-diffusion ability. $\eta(r, t)$ is the thermal noise.[9c] The hydrodynamic effect is neglected throughout as, although they may play an important role in the very late stage of phase separation, the early and intermediate stages should not be affected.[11] In order to study phase separation in a polymer mixture, for F, the FHdG free energy (in units of k_BT) is chosen and is given by eq 2 where χ is the temperature-

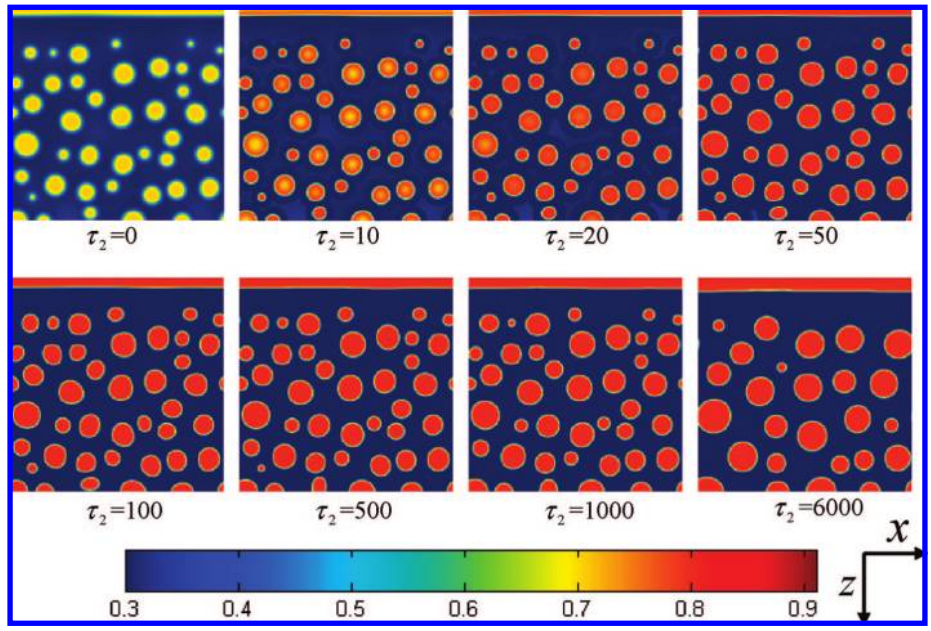

Figure 1. Development of the polymer morphology following a second quench with $\varepsilon_2 = 0.155$, $\varepsilon_1 = 0.06$, and $\phi_0 = 0.4$. The color bar indicates the concentration of the wetting component for the surface.

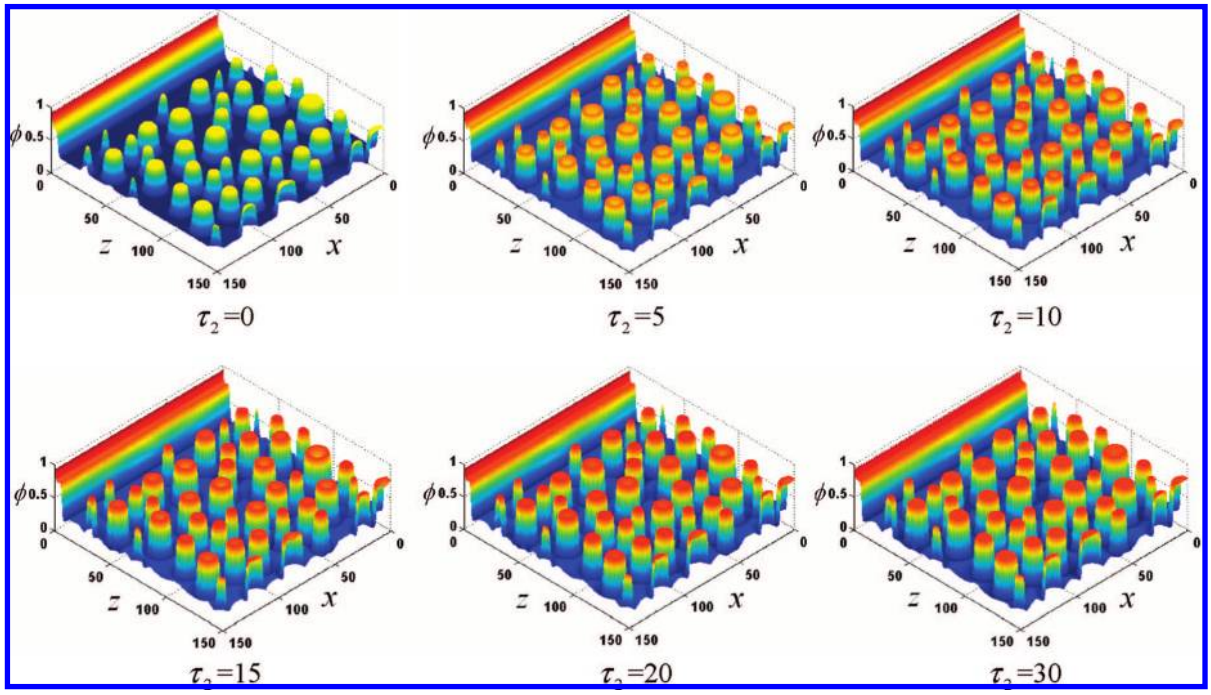

Figure 2. Three-dimensional diagrams showing the concentration fluctuation of secondary domain structures following a second quench with $\varepsilon_2 = 0.155$, $\varepsilon_1 = 0.06$, and $\phi_0 = 0.4$. The color bar is the same as that in Figure 1.

dependent Flory−Huggins dimensionless interaction parameter and b is the Kuhn statistical segment length.[10]

$$F(\varphi) = \int_V \mathrm{d}r\left[\frac{\varphi}{N}\ln(\varphi) + \frac{(1-\varphi)}{N}\ln(1-\varphi) + \chi\varphi(1-\varphi) + \frac{b^2}{36\varphi(1-\varphi)}|\nabla\varphi|^2\right] \quad (2)$$

The integral is performed over the volume, V, of the sample. In terms of the deduction of Puri and Binder,[4c] the boundary conditions of the SDPS dynamic model based on the CHC equation can be described by two partial differential equations. The first equation is defined as eq 3 where h_1, g, and γ are three parameters characterizing the static surface diagram.[4c] h_1 characterizes the surface potential which models the preferences of the surface for one of the components. g characterizes the exchange interaction between sites on the surface in the underlying microscopic model. γ is the parameter which has a relation with the bulk correlation length. z_0 is the location of the surface.

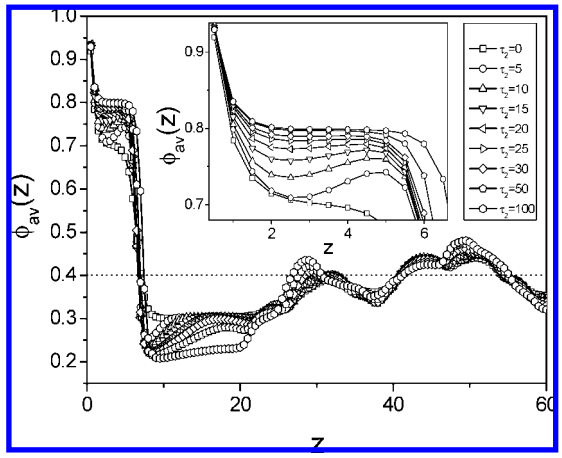

Figure 3. Averaged profiles in the z-direction following a second quench with $\varepsilon_2 = 0.155$, $\varepsilon_1 = 0.06$, and $\phi_0 = 0.4$. The inset indicates the profiles near the surface.

$$\frac{\partial\varphi(x, z_0, \tau)}{\partial\tau} = -h_1 - g\varphi(x, z_0, \tau) + \gamma\frac{\partial\varphi(x, z, \tau)}{\partial z}\bigg|_{z=z_0} \quad (3)$$

A second boundary condition, $\Delta J|_{z=z_0} = 0$, where J, defined as $J = \nabla\delta F/\delta\phi$, is the polymer flux and is used to ensure that the flux of polymer components through the surface boundary is zero, which enforces conservation of the order parameter. In the present study, we choose the z-axis as the direction of the surface effect and consider only one surface located at $z_0 = 0$. It has been proved that the calculated results have more precision if eq 3 is coupled into the dynamic model.[12] Thus, by lumping together eqs 1–3, and by rescaling into a dimensionless form, the dynamic equation can be obtained as follows:

$$\frac{\partial\varphi(\bar{r}, \tau)}{\partial\tau} = \frac{1}{2}\nabla^2\left[\frac{\chi_c}{2(\chi_f - \chi_s)}\ln\frac{\varphi}{1-\varphi} - \frac{2\chi}{\chi_f - \chi_s}\varphi + \frac{2\varphi - 1}{36\varphi^2(1-\varphi)^2}(\nabla\varphi)^2 - \frac{1}{18\varphi(1-\varphi)}\nabla^2\varphi + \left(-h_1 - g\varphi + \gamma\frac{\partial\varphi}{\partial z}\bigg|_{z=0}\right)\delta(z) + \rho\xi(x, \tau) \quad (4)$$

χ_s is the spinodal value of χ at $\phi = \phi_0$, i.e., $\chi_s = 1/[2N\phi_0(1 - \phi_0)]$, where ϕ_0 is the initial average concentration of component A. χ_c is the value of χ at the critical point ($\phi = 0.5$) of the spinodal curve.χ_f is the deepest quench. $\bar{r}$ and τ are rescaled spatial and temporal variables, respectively, given by $\bar{r} = (|\chi_f - \chi_s|)^{1/2}r/l$ and $\tau = NM(\chi_f - \chi_s)^2t/l^2$. $\delta(x)$ is the Dirac δ function, ensuring that the surface free energy only affects the system near $z_0 = 0$. In essence, the surface potential used in the model is short-range because the power law potential, depending on the distance from the surface, is not included in it. It should be noted that the temperature dependent on the mobility is not explicitly considered because the time steps are scaled by the mobility. Hence, the difference between mobility for different quench depths can be reflected in a different scaling factor from numerical time to real time. Importantly, the structural growth is not affected by this assumption.[8b] Equation 4 can be solved using the finite

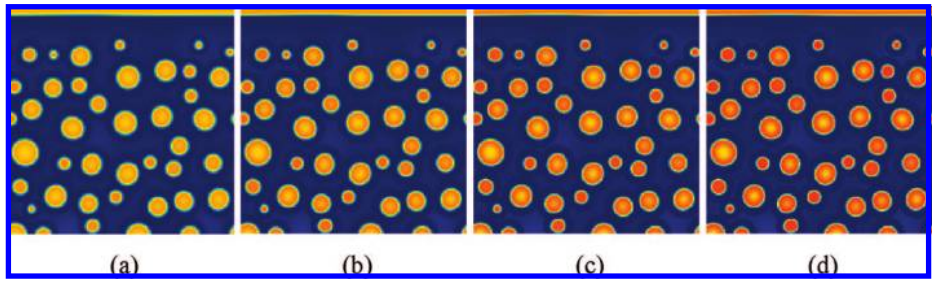

Figure 4. Polymer morphology at $\tau_2 = 10$ and following different second quench depths with $\varepsilon_1 = 0.06$ and $\phi_0 = 0.4$. The color bar is the same as that in Figure 1. (a) $\varepsilon_2 = 0.1$. (b) $\varepsilon_2 = 0.12$. (c) $\varepsilon_2 = 0.14$. (d) $\varepsilon_2 = 0.155$.

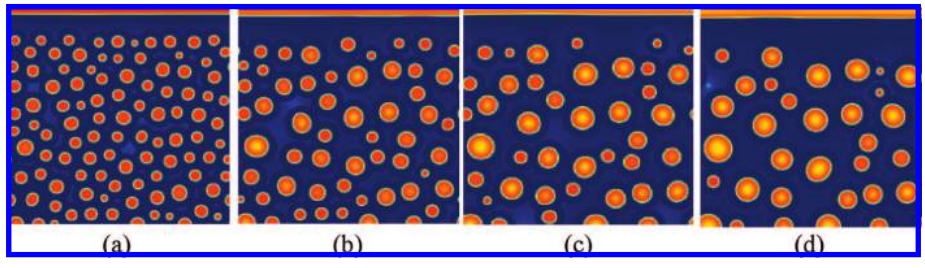

Figure 5. Polymer morphology at $\tau_2 = 10$ and following different first quench times with $\varepsilon_1 = 0.06$, $\varepsilon_2 = 0.155$, and $\phi_0 = 0.4$. The color bar is the same as that in Figure 1. (a) $\tau_1 = 1000$. (b) $\tau_1 = 3000$. (c) $\tau_1 = 5000$. (d) $\tau_1 = 7000$.

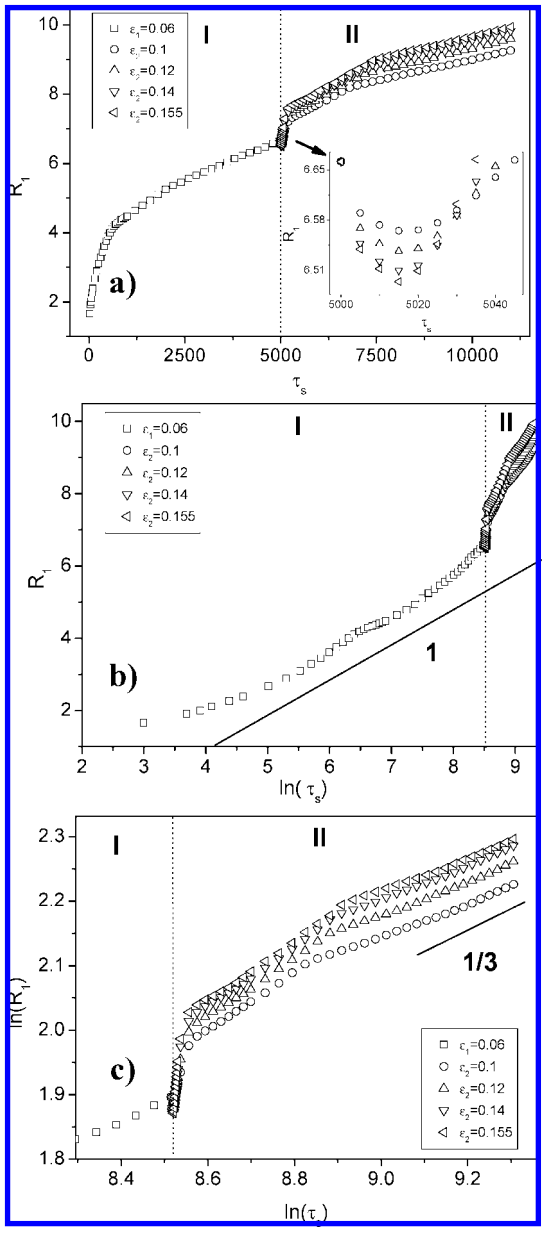

Figure 6. Plots of the wetting layer thickness, R_1, vs the total evolution time τ_s with different values of ε_2 in different scales, where $\varepsilon_1 = 0.06$ and $\phi_0 = 0.4$. (I) The first quench process. (II) The second quench process. (a) In the linear−linear scale. (b) In the linear−ln scale. (c) In the ln−ln scale.

difference approach.[13] Numerically, for the sake of numerical stability and higher accuracy, the Laplacian ∇^2 is discretized based on the cell dynamics scheme (CDS) proposed by Oono and Puri.[14] It is then transformed as[15]

$$\nabla^2 X \rightarrow \frac{1}{\xi^2}(\langle\langle X\rangle\rangle - X) \tag{5}$$

where ξ is the cell size. $\langle\langle X(\bar{r}, \tau)\rangle\rangle$ represents the following summation of $X(\{\bar{r}\})$ for the nearest neighbors ($\bar{r}.$) and the next-nearest neighbors ($\bar{r}.\bar{r}.$):

$$\langle\langle X(\bar{r})\rangle\rangle = B_1 \sum_{\bar{r}=\bar{r}.} X(\bar{r}) + B_2 \sum_{\bar{r}=\bar{r}.\bar{r}.} X(\bar{r}) \tag{6}$$

where B_1 and B_2 are 1/6 and 1/12, respectively. In order to avoid the discretization effect due to the lattice size,[12] the surface terms h_1, g, and γ are rescaled by the step length of the spatial discretization, $\Delta\bar{r}$, and are listed as follows:

$$h_1 \rightarrow h_1/\Delta\bar{r} \qquad g \rightarrow g/\Delta\bar{r} \qquad \gamma \rightarrow \gamma/\Delta\bar{r} \tag{7}$$

Our simulations are carried out on a 300 × 300 two-dimensional lattice. Flat boundary conditions are applied at the other end in the perpendicular direction, and periodic boundary conditions are applied in the parallel direction.[4a–e] Noise, with the magnitude of $\pm 1 \times 10^{-3}$, is only added once at the start of the quench. $h_1 = -1.5$, $g = 0.1$, $\gamma = 0.1$, and $N = 200$ are set in all simulations. To simplify the numerical procedure, and to avoid having to rescale the lattice, $\chi_f - \chi_s$ is chosen to be the same before and after the quench and is fixed at 0.0133 throughout simulations. The Δt (time step) value used during the temporal discretization is 1×10^{-4}, and the spatial discretization step is $\Delta\bar{r} = 0.5$. A dimensionless parameter, ε, which is defined as $\varepsilon = (\chi - \chi_c)/\chi_c$, denotes the quench depth in this work. ε_1 and ε_2 indicate the first and second quench depths, respectively. The first and second quench times are characterized by the parameters of τ_1 andτ_2. The total evolution time was denoted by τ_s and $\tau_s = \tau_1 + \tau_2$.

3. Results and Discussion

For the polymer mixture near a preferential surface, the off-critical condition includes two distinct situations, i.e., the minority component is preferred by the surface and the majority component is preferred by the surface. There are great differences in the bulk phase morphology and the wetting layer formation mechanisms between these two situations, when the mixture is directly quenched from the one-phase region of the phase diagram to a deeper quench depth.[5] When the preferential component is the minority component, the average concentration of the mixture is selected as $\phi_0 = 0.4$. For the other situation $\phi_0 = 0.6$ is chosen. The first quench depth for these two situations is selected as $\varepsilon_1 = 0.06$, in which the phase separation degree is relatively weak.[5] $\tau_1 = 5000$ is selected in these both situations as the end time of the first quench process or the start point of the second quench process excepting special explanation. For simplicity, the phase morphology and evolution dynamics during the first quench process are not listed in this paper, which, however, can be found in our previous work.[5] Different second quench depths ε_2 are selected to examine the effects of the second quench depth on the phase morphology and the wetting layer formation mechanisms.

3.1. Minority Component is Preferred by the Surface. ***3.1.1. Phase Morphology and Evolution Dynamics.*** We would first like to show the formation and evolution of the phase morphology when the minority component is preferred by the surface. Figure 1 illustrates the temporal evolution of the phase morphology when the mixture, with the average concentration $\phi_0 = 0.4$, is quenched from $\varepsilon_1 = 0.06$ to a deeper quench depth with $\varepsilon_2 = 0.155$. The concentration of the preferential component for the surface is marked with the color bar. It can be found that, at the initial time with $\tau_2 = 0$, the polymer mixture exhibits the usual droplet morphology based on the formation mechanism of nucleation and growth in the off-critical phase separation.[16] When a further second quench is applied to this mixture, the concentration in the centers of the particles instantaneously decreases. At the same time, the concentration at the edges of the particles correspondingly increases, leading to the formation of the core−shell structure. One can also note that, at $\tau_2 = 10$, a light concentration drop also occurs in the middle of the wetting layer. With the increasing time, these typical secondary domain structures disappear gradually. The original morphology

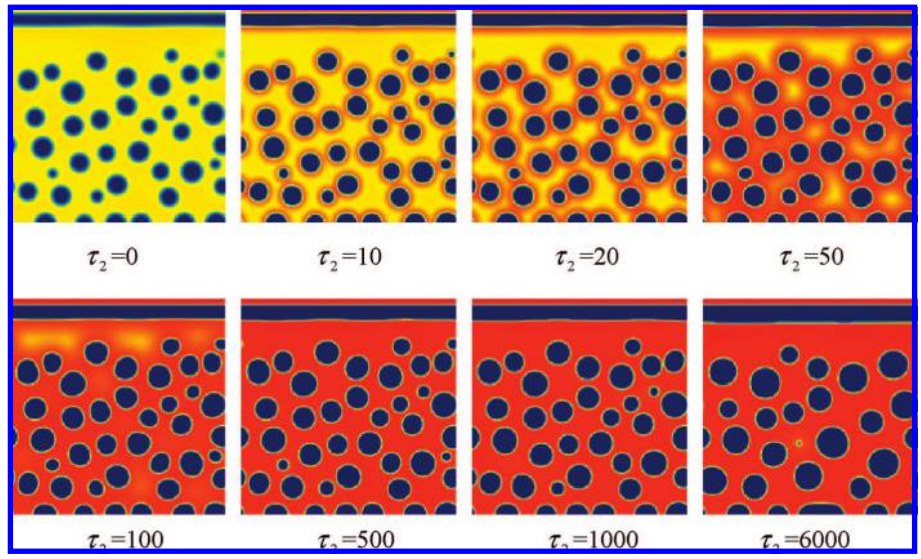

Figure 7. Development of the polymer morphology following a second quench with $\varepsilon_2 = 0.155$, $\varepsilon_1 = 0.06$, and $\phi_0 = 0.6$. The color bar is the same as that in Figure 1.

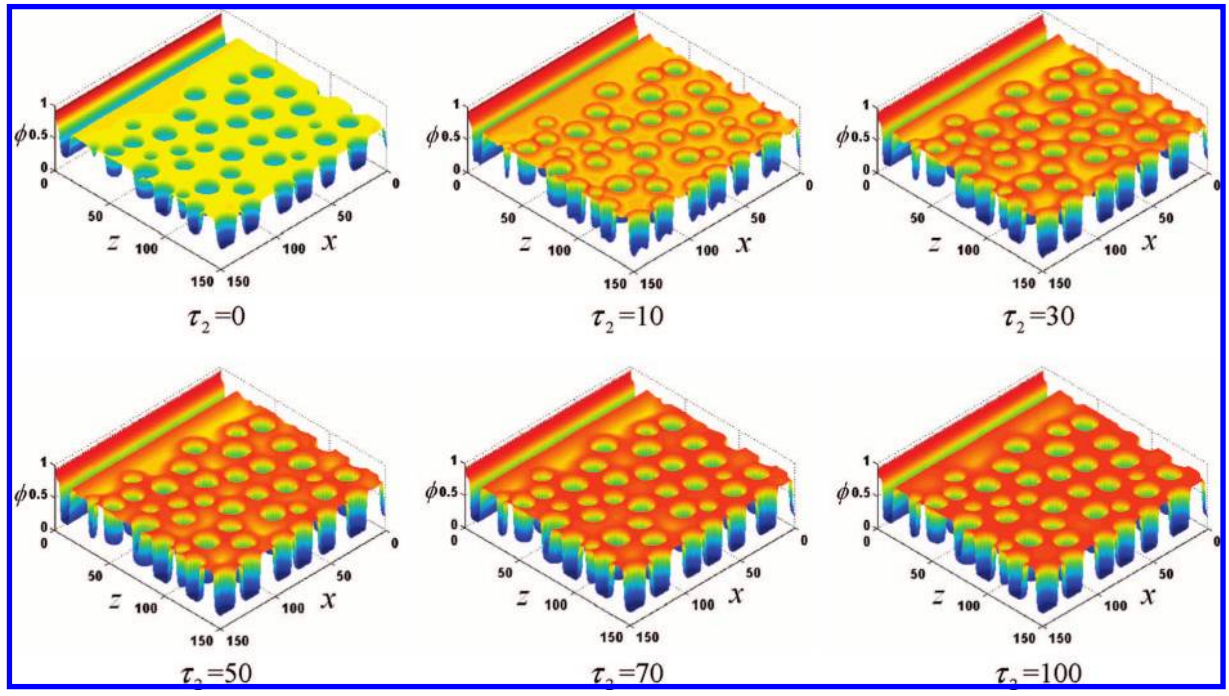

Figure 8. Three-dimensional diagrams showing the concentration fluctuation of secondary domain structures following a second quench with $\varepsilon_2 = 0.155$, $\varepsilon_1 = 0.06$, and $\phi_0 = 0.6$. The color bar is the same as that in Figure 1.

is returned but with higher concentration contrast between two phases until $\tau_2 = 50$. Then, the coalescence of the droplets occurs, and the irregularly anisotropic droplets gradually shrink and reshape into circular ones. With the increasing time, some small droplets shrink and disappear, which leads to the decrease of the total droplet number.

Figure 2 shows the three-dimensional (3D) diagrams of the concentration fluctuation, highlighting a more detailed development of the secondary domain structures. In the 3D diagrams, the cores of the particles and the middle part of the wetting layer fall off when a further second quench is applied to the mixture, demonstrating the formation of the secondary domain structures. These falling parts will ascend again and reach to a new altitude with higher concentration as shown in the patterns from $\tau_2 = 10-30$. It is obvious that the wetting layer and the particles in the bulk undergo extreme concentration fluctuation when the mixture is further quenched to a point in the unstable region of the phase diagram.

The component concentration fluctuation can also be analyzed by the laterally averaged profiles in the z-direction. It can be obtained by averaging the concentration profile $\phi(x, z, \tau)$ of the parallel cross sections along the z-axis as eq 8 for a single run and then ensemble averaging over 10 different runs.

$$\varphi_{av}(z, \tau) = \frac{1}{N_x}\sum_x \varphi(x, z, \tau) \tag{8}$$

where N_x is the total mesh points in each row along the x-direction. Figure 3 shows the plots of the laterally averaged concentration against z at different second quench times with $\varepsilon_2 = 0.155$, $\varepsilon_1 = 0.06$, and $\phi_0 = 0.4$. It can be seen that extreme fluctuation occurs in the bulk during the second quench process.

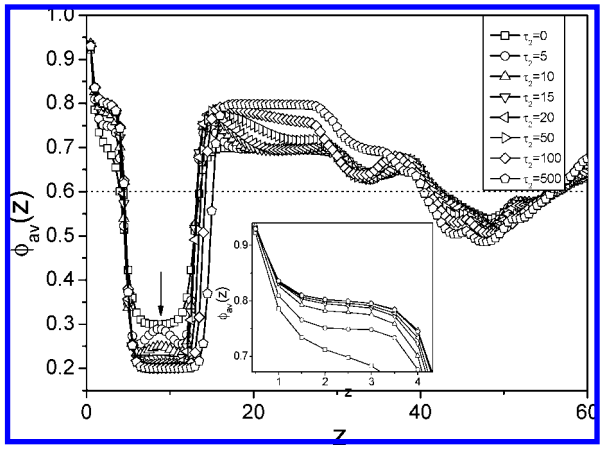

Figure 9. Averaged profiles in the z-direction following a second quench with $\varepsilon_2 = 0.155$, $\varepsilon_1 = 0.06$, and $\phi_0 = 0.6$. The inset indicates the profiles near the surface.

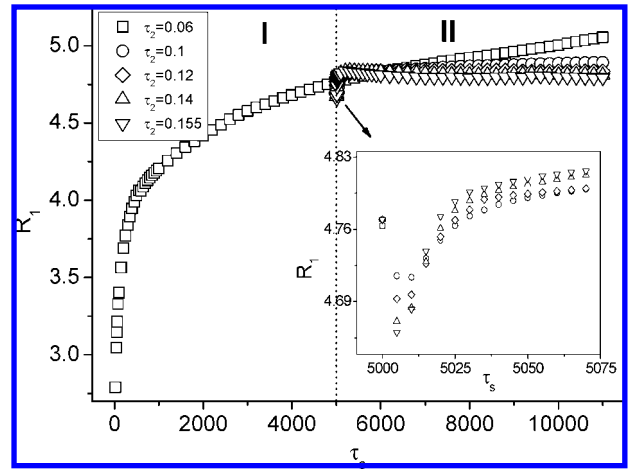

Figure 11. Plots of the wetting layer thickness R_1 vs the total evolution time τ_s with different values of ε_2, where $\varepsilon_1 = 0.06$ and $\phi_0 = 0.6$. (I) The first quench process. (II) The second quench process.

The inset of the figure indicates the profiles near the surface at a large scale. Clearly, the concentration in the middle of the wetting layer falls off at the initial time of the second quench process, corresponding to the formation of the light concentration drop as shown in Figures 1 and 2. With the increasing time, the concentration fluctuation in the wetting layer disappears gradually, representing the observation in the previous figures.

Figure 4 illustrates the polymer morphology at $\tau_2 = 10$ and following different second quench depths with $\varepsilon_1 = 0.06$ and $\phi_0 = 0.4$. It can be found that the typical secondary domain structures in this situation, i.e., the core−shell structure in the bulk and the light concentration drop in the wetting layer, occur in all of the patterns listed in the figure. One can also note that the secondary domain structures with deeper second quench depths are clearer than those with shallower ones. It is really the consequence of the initially favored length scale becoming smaller with the increasing second quench depth.[6−8] On the other hand, a clearer secondary domain structure may be obtained by tuning the initial phase structure of the second quench depth using different methods, e.g., the coarsening time. Figure 5 shows the polymer morphology at $\tau_2 = 10$ and following different first quench times, τ_1, with $\varepsilon_1 = 0.06$, $\varepsilon_2 = 0.155$, and $\phi_0 = 0.4$. The character length of the phase structure increases with the coarsening process during the first quench. One can note that the secondary domain structures will be clearer when the character lengths of the bulk phase structure at the initial stage of the second quench are bigger, corresponding to the previous conclusion.

3.1.2. Growth Dynamics of the Wetting Layer Thickness. The thickness of the surface layer, R_1, can be measured by finding the z-position of the first value of 0.5 in the z-averaged concentration profile. The relationships between the wetting layer thickness and the total evolution time τ_s for both the same first quench depth ($\varepsilon_1 = 0.06$) and various second quench depths with $\phi_0 = 0.4$ are illustrated in Figure 6. Figure 6a−c exhibits the plots in the linear−linear, the linear−ln, and the ln−ln scales, respectively. The inset in Figure 6a indicates the detailed evolution of the wetting layer thickness at the initial stage of the second quench process. It can be found that R_1 instantly decreases when the second further quench is applied. Then, it turns to increase extremely. Moreover, a deeper second quench depth leads to a stronger fluctuation of the wetting layer thickness, corresponding to the previous patterns. In comparison to that in the first quench process, the growth of the wetting layer thickness with a further second quench depth crosses over to a faster growth. The lines in Figure 6, parts b and c, clarify the growth dynamics mechanisms of the wetting layer thickness during these both quench processes. In the first quench process with $\varepsilon_1 = 0.06$ the wetting layer thickness grows logarithmically, i.e., $R_1 \propto \ln(\tau_s)$. However, the evolution of the wetting layer thickness obeys the LS growth law, i.e., $R_1 \propto \tau_s^{1/3}$, in the second quench process. Clearly, the formation mechanism of the wetting layer changes and is finally determined by the second quench depth, which, we think, can promote the understanding on corresponding phenomena observed in the experiments and the technological application of SDPS.[2]

3.2. Majority Component is Preferred by the Surface. ***3.2.1. Phase Morphology and Evolution Dynamics.*** Let us consider the other situation that the majority component is preferred by the surface. Figure 7 illustrates the development of the polymer morphology with $\phi_0 = 0.6$ and a further second quench depth ($\varepsilon_2 = 0.155$). One can find that the droplets of the minority component appear in the bulk at $\tau_2 = 0$. When a further quench is applied, the core−shell particles also form instantly in the bulk. However, in comparison to the core−shell

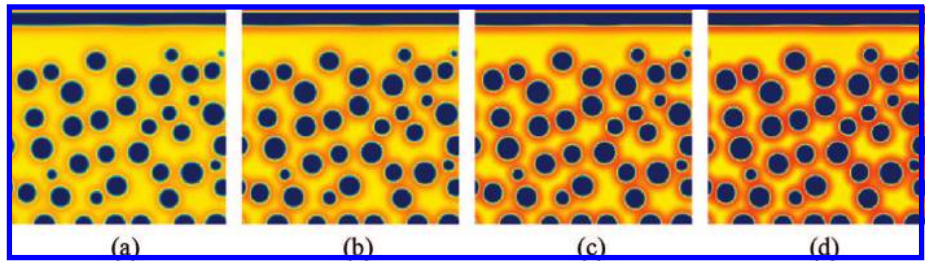

Figure 10. Polymer morphology at $\tau_2 = 20$ and following different second quench depths with $\varepsilon_1 = 0.06$ and $\phi_0 = 0.6$. The color bar is the same as that in Figure 1. (a) $\varepsilon_2 = 0.1$. (b) $\varepsilon_2 = 0.12$. (c) $\varepsilon_2 = 0.14$. (d) $\varepsilon_2 = 0.155$.

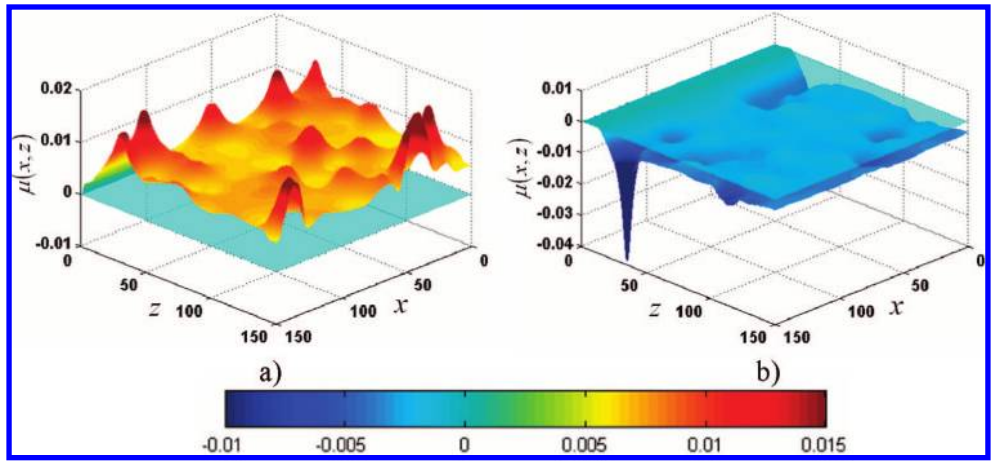

Figure 12. Three-dimensional diagrams showing the chemical potential, $\mu(x, z)$, with $\varepsilon_1 = 0.06$ at $\tau_1 = 5000$. (a) $\phi_0 = 0.4$. (b) $\phi_0 = 0.6$.

structure forming in the situation that the minority component is preferred by the surface, the core in this situation is really the original particles and the shell is the new rich layer of the majority component induced by the second quench. The thickness of the shell for each particle will increase, leading to the connection of one another. The original morphology is returned gradually but with higher concentration contrast between two phases. Then, the coalescence of the droplets occurs, and the irregularly anisotropic droplets gradually shrink and reshape into circular ones. However, the light concentration drop in the wetting layer is not found in this situation, which may be due to the fact that the thickness of the wetting layer is very small.

A detailed process regarding the concentration fluctuation of the secondary domain structure relative to Figure 7 is shown by 3D diagrams in Figure 8. Obviously, when the second quench is applied, the extreme concentration fluctuation occurs around each particle. With the increasing time, the range of the fluctuation will expand and finally cover almost the whole phase region of the majority component. Accordingly, the height contrast between two phases is enlarged. Although the appearance of these secondary domain structures in these both situations of the off-critical condition is brief, we think that they can still be used to tune the phase separation process by appropriate control methods and obtain the interesting phase structures.

Figure 9 plots the laterally averaged concentration against z at different second quench times with $\varepsilon_2 = 0.155$, $\varepsilon_1 = 0.06$, and $\phi_0 = 0.6$. The inset of the figure indicates the profiles near the surface at a large scale. It can be found from the inset that the light concentration drop does not form in the wetting layer, partly because the concentration fluctuation near the surface is weaker than that in the other situation as shown in Figure 4, and partly because the thickness of the wetting layer is very small. The arrow in the figure denotes that the second further quench depth can also induce extreme concentration fluctuation in the depletion layer of the preferential component. The concentration contrast between the depletion layer and the bulk becomes much larger with the increasing time.

The phase structures at $\tau_2 = 20$ and following different second quench depths with $\phi_0 = 0.6$ and $\varepsilon_1 = 0.06$ are exhibited in Figure 10. It can be seen that the core−shell structure as shown in Figure 7 also appears in these patterns with different second quench depths. One can note that the secondary domain structure with the deeper second quench depth is clearer than that with the shallower one, demonstrating again that a deeper second quench depth can induce a more intensive concentration fluctuation and a smaller initially favored length scale, corresponding to Figure 4.

3.2.2. Growth Dynamics of the Wetting Layer Thickness. Figure 11 illustrates the temporal evolution of the wetting layer thickness R_1 during the first quench process with $\varepsilon_1 = 0.06$ and the second one with different ε_2. The inset indicates the detailed evolution of the wetting layer thickness at the initial stage of the second quench process. Our previously simulated results have demonstrated that the evolution of the wetting layer thickness really obeys a logarithmic growth law in the first quench process.[5] When the second deeper quench is applied, one can note from the inset that R_1 instantaneously decreases. Then, it returns quickly to almost the original value. Moreover, a deeper second quench depth leads to a stronger fluctuation of the wetting layer thickness, reproducing the observation for the previous patterns. However, the growth of the wetting layer thickness in the second quench process gets slow and a deeper second quench depth corresponds to a slower growth, which are contrary to those in the other situation as shown in Figure 6. Clearly, the growth of the wetting layer thickness does not obey a logarithmic growth law in the second quench process. It can also be found that the wetting layer thickness at a certain time decreases in the second quench process when the quench depth gets deeper, which is also contrary to that illustrated in Figure 6.

How can we understand these differences regarding the growth of the wetting layer thickness in these two situations? To answer the question in depth, the chemical potential, $\mu_b(x, y, z)$, based on the preferential component is considered and can be calculated as follows:[1]

$$\mu_b = \frac{1}{N(\chi_f - \chi_s)} \ln \frac{\varphi}{1-\varphi} - \frac{2\chi}{\chi_f - \chi_s}\varphi + \frac{2\varphi - 1}{36\varphi^2(1-\varphi)^2}(\nabla\varphi)^2 - \frac{1}{18\varphi(1-\varphi)}\nabla^2\varphi + \left(-h_1 - g\varphi + \gamma\frac{\partial\varphi}{\partial z}\Big|_{z=z_0}\right)\delta(z) \quad (9)$$

For the convenience to compare the difference between the chemical potential in both situations of the off-critical condition, the value of the chemical potential in each lattice is reduced by that near the surface, leading to the relative chemical potential, $\mu(x, z)$. In Figure 12 are 3D diagrams showing the fluctuation of the chemical potential at the initial stage of the second quench

process. It can be found from Figure 12a that, when the minority component is preferred by the surface, the chemical potential in the bulk is higher than that near the wetting layer. However, as shown in Figure 12b, the chemical potential in the bulk is lower than that near the wetting layer in the other situation. Thus, in the first situation, the preferred component in the droplets will feed to the wetting layer. So, in this case, a deeper quench depth can lead to a thicker wetting layer at a certain time and an earlier crossover, which is followed by a faster growth, corresponding to our numerically simulated results in Figure 6. However, in the second situation, the droplets do not supply the preferred component to the wetting layer. On the contrary, due to the difference of the chemical potential between the surface and the bulk, they actually attract the preferred component and should slow down the growth of the wetting layer, corresponding to the results in Figure 11. Moreover, a deeper quench depth can lead to a thinner wetting layer at a certain time, reproducing our simulated result in Figure 11. Clearly the wetting layer formation mechanism is determined by the interplay between the surface potential and the bulk chemical potential. Moreover, the formation dynamics of the wetting layer can be changed by tuning these two potentials using different parameters such as τ_1,[17a] h_1,[17b] and so on.

4. Conclusions

In this paper we numerically concern the two-step SDPS in asymmetry polymer mixtures by coupling the FHdG equation with the CHC equation. The morphology and evolution dynamic of the phase structure, especially the secondary domain structure, are analyzed in detail. The wetting layer formation mechanisms during the two-step quench process are also examined. The simulated results demonstrate that a core−shell structure in the bulk and a light concentration drop in the wetting layer can be induced by the second quench with deeper quench depth, when the minority component is preferred by the surface. When the minority component is preferred by the surface, the second further quench can also induce a core−shell structure. However, the morphologies of the core−shell structures forming in these two situations are different. It is also found that the growth of the wetting layer thickness with further second quench depth can cross over to a faster growth when the preferential component is the minority component. In this situation, the formation mechanism of the wetting layer will change and is eventually determined by the second quench depth. However, when the preferential component is the majority component, the growth of the wetting layer thickness in the second quench process gets slow and a deeper second quench depth corresponds to a slower growth. The chemical potential can be used to explain the difference regarding the growth dynamics of the wetting layer thickness between these both situations.

Acknowledgment. Financial support from the National Natural Science Foundation of China (Nos. 90103035, 20174022, and 10334020) is highly appreciated. L.-T.Y. acknowledges the Alexander von Humboldt Foundation for support.

References and Notes

(1) (a) Binder, K. *Adv. Polym. Sci.* **1989**, *138*, 1. (b) Bray, A. J. *Adv. Phys.* **1994**, *43*, 357. (c) Furukawa, H. *Adv. Phys.* **1985**, *37*, 703.

(2) For reviews of experimental studies of this problem, see: (a) Geoghegan, M.; Krausch, G. *Prog. Polym. Sci.* **2003**, *28*, 261. For reviews of numerical simulations of this problem, see: (b) Puri, S.; Frisch, H. L. *J. Phys.: Condens. Matter* **1997**, *9*, 2109. (c) Puri, S. *J. Phys.: Condens. Matter* **2005**, *17*, R101.

(3) (a) Jones, R. A. L.; Norton, L.; Kramer, E. J.; Bates, F. S.; Wiltzius, P. *Phys. Rev. Lett.* **1991**, *66*, 1326. (b) Krausch, G.; Dai, C.-A.; Kramer, E. J.; Marko, J. F.; Bates, F. S. *Macromolecules* **1993**, *26*, 5566. (c) Geoghegan, M.; Ermer, H.; Jungst, G.; Krausch, G.; Brenn, R. *Phys. Rev. E* **2000**, *62*, 940. (d) Sung, L.; Karim, A.; Douglas, J. F.; Han, C. C. *Phys. Rev. Lett.* **1996**, *76*, 4368. (e) Wang, W.; Shiwaku, T.; Hashimoto, T. *Macromolecules* **2003**, *36*, 8088.

(4) (a) Puri, S.; Binder, K. *Phys. Rev. A* **1992**, *46*, R4487. (b) Puri, S.; Binder, K. *Phys. Rev. E* **1994**, *49*, 5359. (c) Puri, S.; Binder, K. *Phys. Rev. E* **1997**, *56*, 6991. (d) Puri, S.; Binder, K. *Phys. Rev. Lett.* **2001**, *86*, 1797. (e) Puri, S.; Binder, K. *Phys. Rev. E* **2002**, *66*, 061602. (f) Marko, J. F. *Phys. Rev. E* **1993**, *48*, 2861. (g) Toxvaerd, S. *Phys. Rev. Lett.* **1999**, *83*, 5318. (h) Rysz, J. *Polymer* **2005**, *46*, 977.

(5) Yan, L.-T.; Xie, X.-M. *J. Chem. Phys.* **2007**, *126*, 064908.

(6) (a) Hashimoto, T.; Hayashi, M.; Jinnai, H. *J. Chem. Phys.* **2000**, *112*, 6886. (b) Hayashi, M.; Jinnai, H.; Hashimoto, T. *J. Chem. Phys.* **2000**, *112*, 6897. (c) Hayashi, M.; Jinnai, H.; Hashimoto, T. *J. Chem. Phys.* **2000**, *113*, 3414.

(7) (a) Tanaka, H. *Phys. Rev. E* **1993**, *47*, 2946. (b) Sigehuzi, T.; Tanaka, H. *Phys. Rev. E* **2004**, *70*, 051504. (c) Rullmann, M.; Alig, I. *J. Chem. Phys.* **2004**, *120*, 7801.

(8) (a) Clarke, N. *Phys. Rev. Lett.* **2002**, *89*, 215506. (b) Henderson, I. C.; Clarke, N. *Macromolecules* **2004**, *37*, 1952. (c) Fialkowski, M.; Holyst, R. *J. Chem. Phys.* **2002**, *117*, 1886.

(9) (a) Cahn, J. W.; Hilliard, J. E. *J. Chem. Phys.* **1958**, *28*, 258. (b) Cahn, J. W. *J. Chem. Phys.* **1965**, *42*, 93. (c) Cook, H. E. *Acta Metall.* **1970**, *18*, 297.

(10) (a) Flory, P. J. *Principles of Polymer Chemistry*; Cornell University Press: Ithaca, NY, 1953. (b) de Gennes, P. G. *J. Chem. Phys.* **1980**, *72*, 4756.

(11) Tanaka, H. *J. Phys.: Condens. Matter* **2001**, *13*, 4637.

(12) Henderson, I. C.; Clarke, N. *Macromol. Theory Simul.* **2005**, *14*, 435.

(13) Glotzer, S. C. *Annu. Rev. Comput. Phys.* **1995**, *2*, 1.

(14) (a) Oono, Y.; Puri, S. *Phys. Rev. A* **1988**, *38*, 434. (b) Puri, S.; Oono, Y. *Phys. Rev. A* **1988**, *38*, 1542.

(15) Ohta, T.; Enomoto, Y.; Harden, J. L.; Doi, M. *Macromolecules* **1993**, *26*, 4928.

(16) (a) Nakai, A.; Wang, W.; Ogasawara, S.; Hasegawa, H.; Hashimoto, T. *Macromolecules* **1996**, *31*, 5391. (b) Wang, X.; Okada, M.; Matsushita, Y.; Furukawa, H.; Han, C. C. *Macromolecules* **2005**, *38*, 7127.

(17) (a) Yan, L.-T.; Xie, X.-M. *J. Chem. Phys.* **2008**, *128*, 034901. (b) Yan, L.-T.; Xie, X.-M. *Polymer* **2006**, *47*, 6472. (c) Yan, L.-T.; Xie, X.-M. *J. Chem. Phys.* **2008**, *128*, 154702.

JP801648T